

# Tempo and Mode of Evolutionary Radiation in Iguanian Lizards

Luke J. Harmon, James A. Schulte II, Allan Larson, Jonathan B. Losos

## Supporting Online Material

### Materials and methods

Phylogenies were constructed using an approximately 1800 base-pair mitochondrial DNA region from the protein-coding regions ND1 to COI including the complete ND2 gene, the origin of light-strand replication, and eight tRNAs (tRNA<sup>Ile</sup>, tRNA<sup>Gln</sup>, tRNA<sup>Met</sup>, tRNA<sup>Trp</sup>, tRNA<sup>Ala</sup>, tRNA<sup>Asn</sup>, tRNA<sup>Cys</sup>, tRNA<sup>Tyr</sup> [*S1*, *S2*, *S3*, *S4*, *S5*]). All sequences have been deposited in GenBank (Table S1). Sequences were aligned manually for protein-coding regions and by secondary structural models for tRNAs. For the phrynosomatines, sequences of an additional 17 species were obtained from the mitochondrial DNA region of 12S and 16S (*S6*). Tree reconstructions are based on maximum-likelihood analyses using the GTR+I+ $\Gamma$  model of sequence evolution on the basis of hierarchical hypothesis-testing of alternative models with Modeltest 3.06 (*S7*). All phylogenetic hypotheses were generated using PAUP\* beta version 4.0b10 (*S8*). Phylogenies contained 40-87% of the species in that clade (Table 1) and sampled all major clades; missing species are likely to be relatively closely related to species included in the phylogeny and hence the deep phylogenetic structure of the clades is unlikely to be affected by missing taxa. For *Anolis*, we restricted our analysis to Caribbean species. Trees with branch lengths were estimated using maximum likelihood without assuming a molecular clock. Branch lengths were then scaled proportional to

time using nonparametric rate smoothing (*S9*) as implemented in the program TreeEdit (*S10*).

We measured continuous variables for these lizards pertaining to the limbs, girdles, head and tail, as well as snout-vent length. In addition, for *Anolis*, we included the number of subdigital lamellae under the third and fourth phalanges of pedal digit IV and mass. We measured a majority of the species included in the phylogenetic analyses (65 *Liolaemus*, 69 phrynosomatines, 73 *Anolis*, and 57 Australian agamids). Data were log-transformed prior to all analyses. For each clade, dimensionality of the data was reduced using a principal-components analysis (PCA) on the correlation matrix of the original data. The first four principal components, which accounted for at least 96% of variation in all clades, were retained. In all cases, measurements were taken on adult males. For most species, at least two individuals were measured, from which species mean values were calculated. Characters showed approximately equal coefficients of variation among clades, with *Anolis* exhibiting the most variability and *Liolaemus* the least (Table S2).

We performed null model analyses of the relationship between LDI and MDI to investigate how likely the observed correlation between LDI and MDI is to occur by chance. We simulated both phylogenetic trees and morphological characters to create 1000 random four-clade data sets; within each data set, the four simulated clades corresponded to the four real clades in our analysis. For each simulated data set, trees were simulated using a birth-death process, with the total number of taxa in each tree equal to the number included in the phylogeny we used for our analysis (*S11*; Table 1). For the morphological analysis, these trees were randomly pruned to contain the same number of taxa as were included in our morphological analysis (*S11*), and character

evolution was simulated on those trees under a Brownian-motion model. Thus, the simulated phylogenies for each clade contained the same number of species and with the same morphological variance as the four real clades in our analysis (Table 1). For each simulation for each clade, we calculated the MDI and LDI statistic as described above. In only 4 of 1000 simulations was the absolute value of the correlation between LDI and MDI greater than that observed in the real data ( $p = 0.004$ ).

We also conducted similar analyses using the real phylogenies from our analyses and the LDI statistics calculated for them, but simulating morphological character evolution on these phylogenies. In these analyses, we obtained correlation values for the MDI – LDI relationship greater in magnitude than that actually observed in only 0.3% of the simulations.

We used simulations to determine the effect of incomplete sampling on the MDI statistic. Since we do not know the morphologies of species not included in our study, we could not determine their effect on the MDI statistic. Instead, we conducted 100 simulations which used the species we have included as a starting point, and randomly sampled them so that the proportion of species included was the same as the proportion of species used in our morphological analyses compared to the total number of species in the phylogeny (e.g., we had morphological data for 82.6% of the species in our phylogeny for Australian agamids; thus, in the simulations, we randomly eliminated 10 of 57—17.5%—species). These 100 simulations started from the original phylogenetic tree for each clade and then randomly pruned species until the tree was of the desired size. We then calculated an MDI statistic for each pruned tree using the same methods outlined in the main text of this report, but only including those species not pruned from the tree. To determine what effect, if any, such incomplete sampling had on the MDI - LDI

correlation, we regressed the mean pruned MDI for each clade from the simulations on the original LDI values. As with the original data, the correlation was significantly negative ( $r = -0.98$ ,  $p = 0.02$ ). This suggests that our conclusion, that LDI and MDI are negatively correlated, is robust to incomplete sampling of morphology.

## Supporting figures

Fig. S1. Hypothetical phylogeny of 8 species (A), showing how disparity is calculated.

The first branching event breaks the clade into two subclades, numbered 2 and 3 (B).

Disparity is calculated for each subclade and expressed as a ratio relative to disparity of the entire clade (A). The next speciation event (C) results in lineages defining three subclades: 2, 4, and 5. Relative disparity is calculated for each, and, in a similar fashion, for the four subclades in the bottom right (D). Relative disparity for each time period is calculated by averaging over all subclades whose ancestral lineage was present at that time.

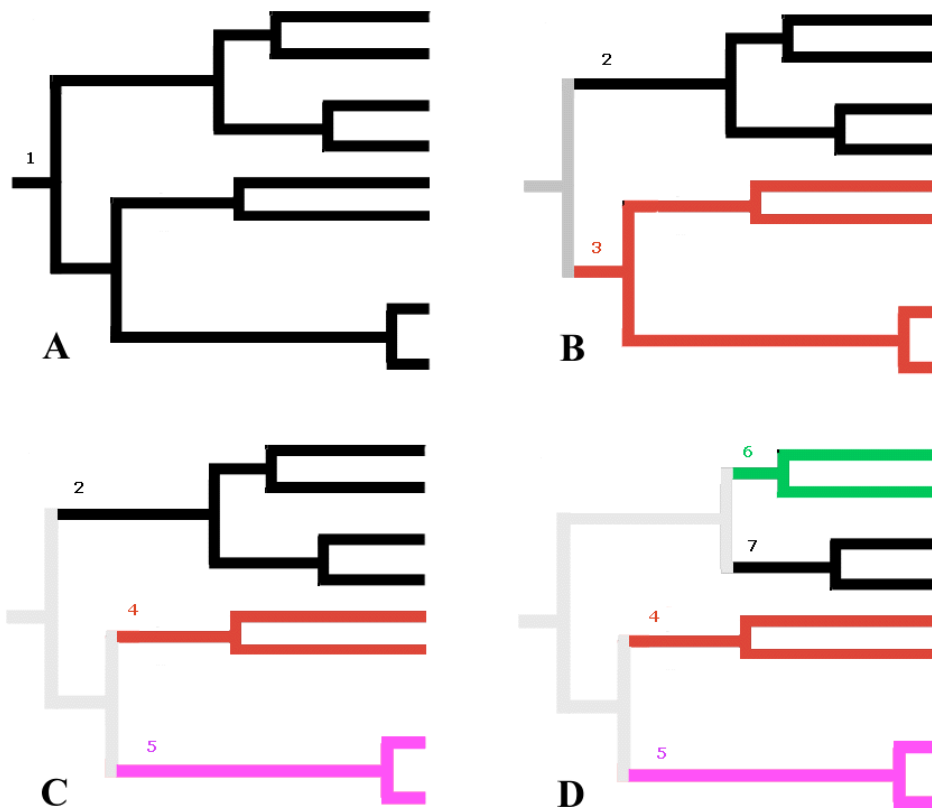


Figure S2. Disparity pattern i. This example illustrates a case in which subclades contain large amounts of variation relative to the entire clade. Colors represent the clade coloring as above. The figure indicates that subclades have diversified extensively and have high values of relative disparity. Subclades overlap substantially in a two-dimensional morphological space, which indicates that species have evolved to fill similar regions of morphological space.

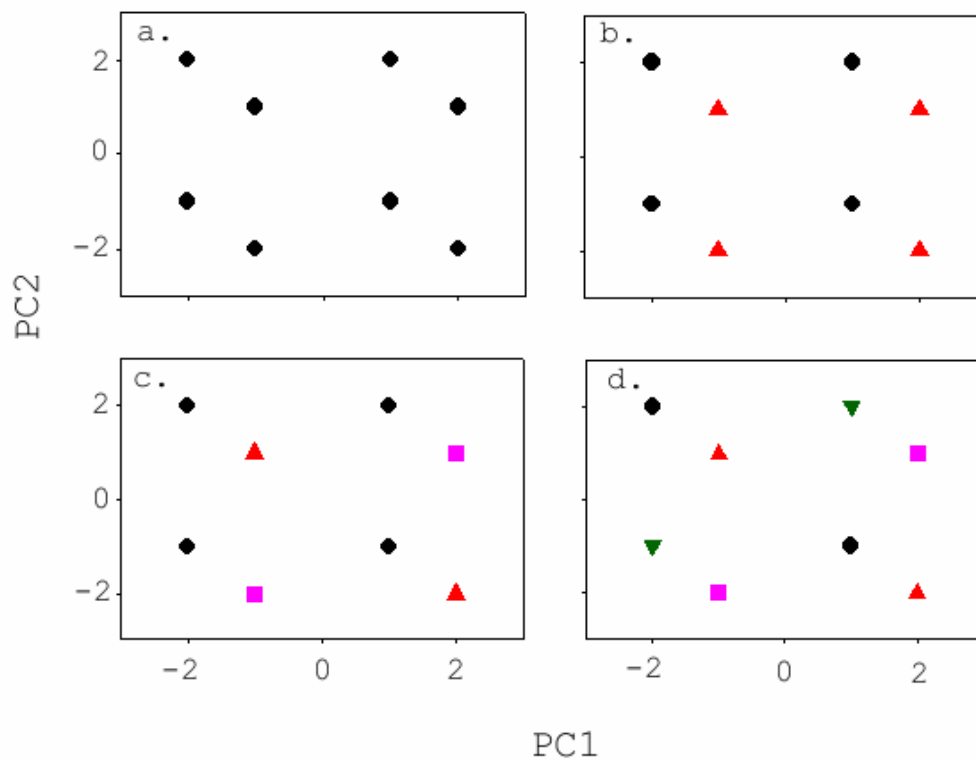


Fig. S3. Disparity pattern ii. By contrast, variation is partitioned among subclades. Each subclade diversifies little and thus has low relative disparity. Little or no overlap exists among subclades.

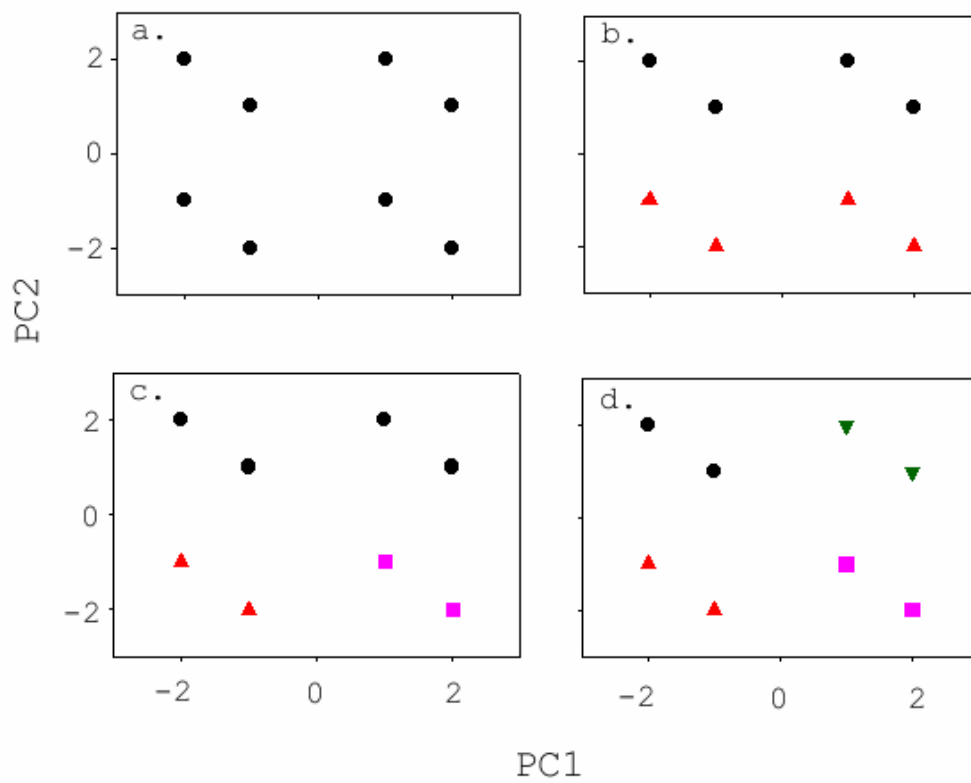


Fig. S4. Relative disparity plot for patterns i and ii. This plot illustrates average relative disparity of subclades versus time for the two patterns shown above. Clearly, pattern i has higher average relative disparity through time, indicating the great variation within subclades and the greater overlap between subclades. The four points for each pattern correspond to the stages of the phylogeny discussed above.

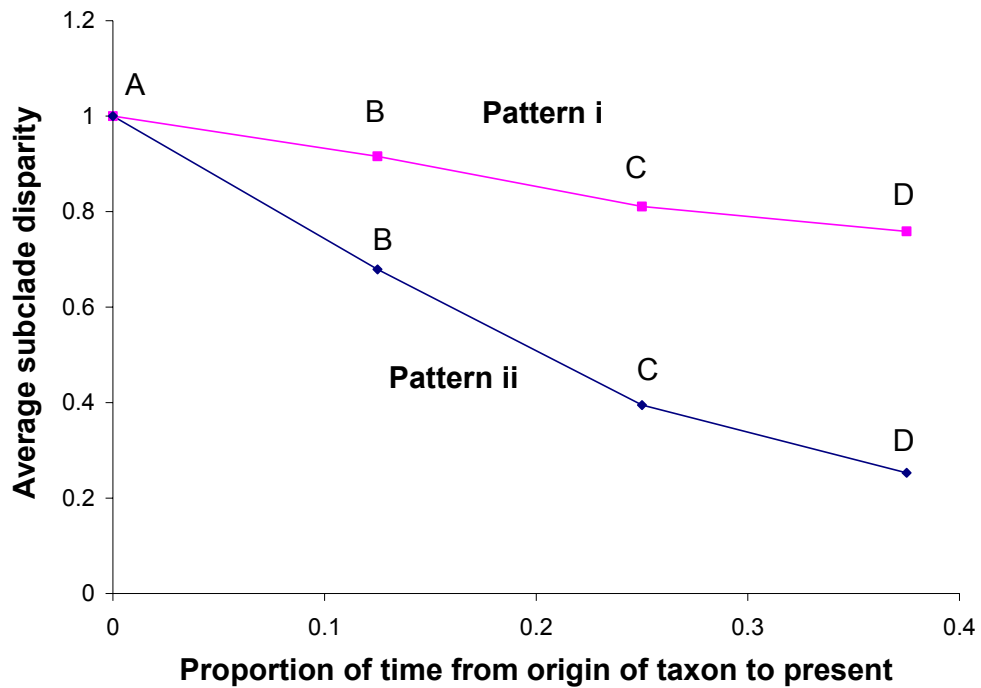


Figure S5. Relationship of LDI and MDI assuming a speciation model of character evolution. For each clade, 1000 morphological data sets were simulated on a phylogeny with the same topology as the tree used in the analysis in Figure 2, but with the expected amount of change equal on all branches of the phylogeny (i.e., a speciation model of character evolution). These data sets were then used to generate disparity-through-time plots, as above, and these plots were then used as a null model for the disparity analysis. We calculated the area between the original data and the median of the null simulations. The results of this analysis are presented below, where they are compared to the results from the gradual analysis from Figure 3; the original, gradual model results are in black, while the speciation model results are in purple. Although changing the null model altered the calculated disparity index for all four clades, the relationship between LDI and MDI was still strongly negative ( $r^2 = 0.91$ ,  $p < 0.05$ ).

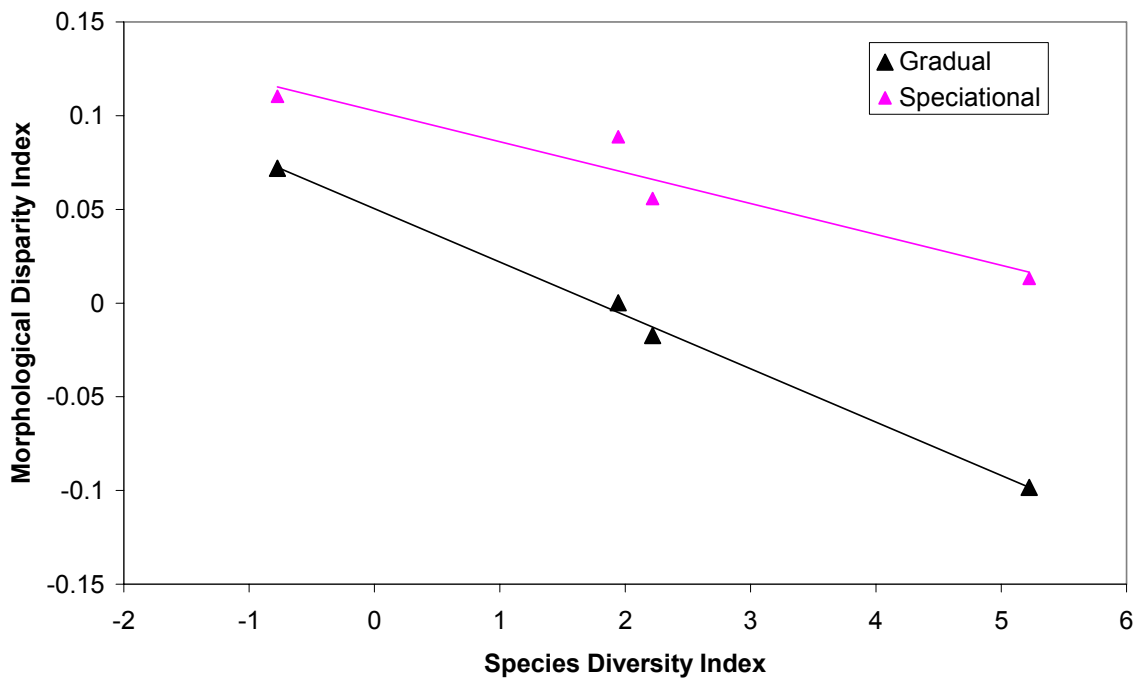


Figure S6. Effect of extinction on diversity patterns. To investigate the effect of departures from a pure-birth model on the lineage diversity index (LDI), we used parametric bootstrapping to construct distributions of LDI statistics for each of the four clades under various models of speciation and extinction. To do this, we simulated phylogenies using the program PhyloGen (*SI1*). For each clade, every simulation had the same net diversification rate, but we used three different extinction rates: no extinction (equivalent to the original analysis presented in figure 1), extinction rate equal to half of the net diversification rate, and extinction rate equal to the net diversification rate. In these simulations, probability of extinction of all lineages was equal. We created 1000 simulated data sets per extinction rate per clade, producing phylogenies to match the total number of known species in the clade. We used these simulated phylogenies to create lineage-through-time plots, which were standardized to a relative time scale as in Figure 1. To create the parametric bootstrapped distribution of LDI statistics, we generated a set of 1000 LDI statistics from these simulated phylogenies. We used these simulations as null models (just as the pure birth model is the null model in Figure 1) and for each one calculated the area between the simulated data set and the actual lineage-through-time plot for that clade, using only the first 2/3 of the phylogeny. The means for these bootstrapped distributions of areas are plotted below and show that at any extinction rate, the expected ordering of the four clades does not change.

At each extinction level, we also used parametric bootstrapping to calculate a distribution of correlation coefficients for the LDI – MDI relationship. To do this, we used the simulations just described. For each set of simulations of the four clades, we regressed the calculated LDI value on the MDI values for each clade. For each regression, we calculated the correlation coefficient ( $r$ ), thus generating a bootstrapped

distribution of correlation coefficients for each level of extinction. We used these distributions to calculate a p-value, which was the number of simulations producing correlations  $\geq 0$  divided by 1000. This p-value can be converted (by subtracting from 1 and multiplying by 100%) to the smallest one-sided confidence interval on  $r$  that would include zero; if this confidence interval exceeds 95%, then the analysis would provide significant support for a negative relationship between LDI and MDI. This test showed significantly negative correlations between MDI and LDI for each level of extinction (extinction = 0,  $p = 0.015$ ; extinction = 0.5 \* net diversification rate,  $p = 0.012$ ; extinction = 1.0 \* net diversification rate,  $p = 0.001$ ).

For a more conservative test incorporating variability in extinction rates among the four clades, we generated another parametrically-bootstrapped distribution of correlation coefficients by randomly selecting an extinction rate for each clade independently (extinction = 0, 0.5, or 1.0 \* net diversification rate). The significance-testing procedure was then the same as in the previous analysis, which used the same extinction rate for all clades. This result was also significant ( $p = 0.009$ ). Thus, our results for the correlation between MDI and LDI are robust to departures from the assumptions of a pure birth model.

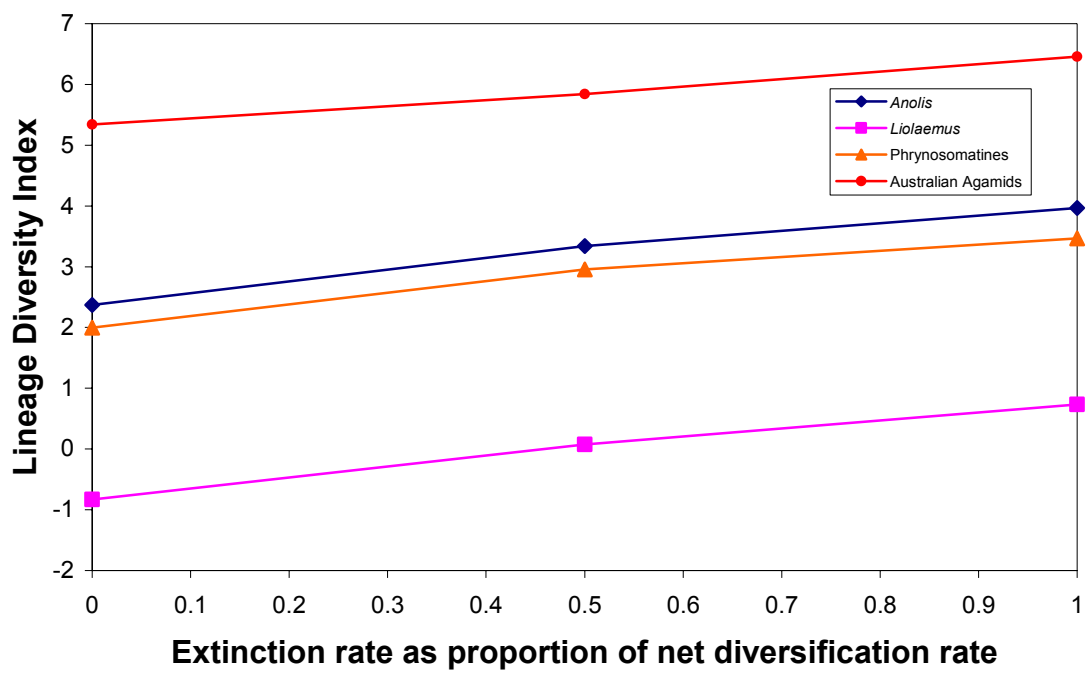
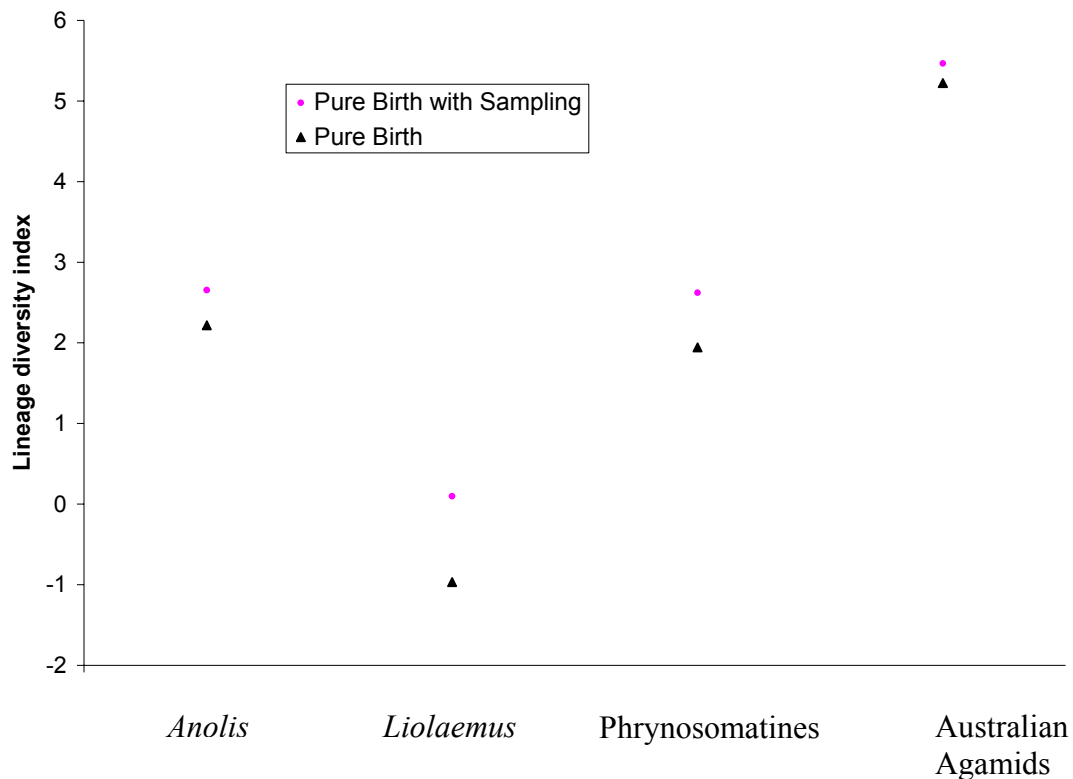


Figure S7. Effect of sampling on diversity patterns. To investigate the effect of incomplete sampling on the lineage diversity index, we generated parametrically-bootstrapped distributions of the LDI values for the four clades that included both stochasticity in the birth process and incomplete sampling. For this analysis, we simulated and resampled phylogenies using the program PhyloGen (Rambaut 2002). For each clade, we simulated phylogenies using a pure-birth model, creating 1000 simulated data sets per clade. We simulated phylogenies to match the total number of known species in the clade, and then randomly selected taxa to exclude until the phylogeny contained the same number of species that were actually sampled in this study. For example, for the agamid clade, we first simulated trees with 79 species and then randomly chose 10 species to be excluded, creating trees of 69 species. We used these simulated phylogenies to create lineage-through-time plots, which were standardized to a relative time scale. As in figure S6, we used these simulations to generate a bootstrapped distribution of LDI statistics for each clade, considering the simulated data sets as a null model that accounts for differences in the completeness of sampling among the groups and stochasticity in the birth process. We generated this null distribution by calculating the area between each simulated data set and the reconstructed lineage-through-time plot for that clade using only the first 2/3 of the phylogeny. The means for these distributions of areas are plotted below and compared to the pure-birth analysis in Figure 1, with the original, pure-birth results in black and the results corrected for incomplete sampling in purple. Correcting for incomplete sampling did not affect the expected order of the four clades on the lineage diversity axis. Furthermore, the negative correlation between the morphological disparity index and this corrected lineage diversity index is still significant (parametric bootstrap, probability value calculated as in Figure S6,  $p = 0.012$ ).

This null model correcting for sampling is conservative because it assumes that every lineage is equally likely to be excluded from the data set. If all unsampled species occur on branches in the last 1/3 of the tree, then sampling would not affect the results presented in Figure 1, because those branches are not incorporated into the analysis. The null model here assumes, by contrast, that species are excluded randomly, in which case many branches would occur in the first 2/3 of the tree. For our data, due to the process of taxon selection, most unsampled species have close relatives that are included in our sampling; consequently, most branches leading to unsampled species probably occurred in the most recent 1/3 of the tree and as a result, the two models presented here bracket the range of possibilities resulting from species sampling.



## Supporting tables

Table S1. GenBank accession numbers for all sequences used in this study. Newly published sequences are those with no reference listed.

<b>Taxon</b>	<b>Species</b>	<b>Accession Number</b>	<b>Reference</b>
<b>Australian agamids</b>	<i>Amphibolurus muricatus</i>	AF128468	S12
	<i>Amphibolurus nobbi</i>	AY132999	S4
	<i>Amphibolurus nobbi coggeri</i>	AY133000	S4
	<i>Amphibolurus norrisi</i>	AY133001	S4
	<i>Amphibolurus temporalis</i>	AY133002	S4
	<i>Caimanops amphiboluroides</i>	AF128472	S12
	<i>Chelosania brunnea</i>	AF128465	S12
	<i>Chlamydosaurus kingii</i>	AF128469	S12
	<i>Ctenophorus adelaidensis</i>	AF128471	S12
	<i>Ctenophorus caudicinctus</i>	AF375623	S3
	<i>Ctenophorus clayi</i>	AF375620	S3
	<i>Ctenophorus cristatus</i>	AF375622	S3
	<i>Ctenophorus decresii</i>	AF128470	S12
	<i>Ctenophorus femoralis</i>	AF375627	S3
	<i>Ctenophorus fionni</i>	AF375638	S3
	<i>Ctenophorus fordi</i>	AF375626	S3
	<i>Ctenophorus gibba</i>	AF375625	S3
	<i>Ctenophorus isolepis</i>	AF375629	S3
	<i>Ctenophorus maculatus</i>	AF375628	S3
	<i>Ctenophorus maculosus</i>	AF375621	S3
	<i>Ctenophorus mckenziei</i>	AF375631	S3
	<i>Ctenophorus nuchalis</i>	AF375633	S3
	<i>Ctenophorus ornatus</i>	AF375624	S3
	<i>Ctenophorus pictus</i>	AF375635	S3
	<i>Ctenophorus reticulatus</i>	AF375634	S3
	<i>Ctenophorus rubens</i>	AF375630	S3
	<i>Ctenophorus rufescens</i>	AF375636	S3
	<i>Ctenophorus salinarum</i>	AF375640	S3
	<i>Ctenophorus scutulatus</i>	AF375632	S3
	<i>Ctenophorus tjantjalka</i>	AF375637	S3
	<i>Ctenophorus vadrappa</i>	AF375639	S3
	<i>Diporiphora albilabris</i>	AY133003	S4

<b>Taxon</b>	<b>Species</b>	<b>Accession Number</b>	<b>Reference</b>
<b>Australian agamids</b>	<i>Diporiphora arnhemica</i>	AY133004	S4
	<i>Diporiphora australis</i>	AY133005	S4
	<i>Diporiphora bennettii</i>	AY133006	S4
	<i>Diporiphora bilineata</i>	AF128473	S12
	<i>Diporiphora lalliae</i>	AY133007	S4
	<i>Diporiphora lingua</i>	AY133008	S4
	<i>Diporiphora magna</i>	AY133009	S4
	<i>Diporiphora pindan</i>	AY133010	S4
	<i>Diporiphora reginae</i>	AY133011	S4
	<i>Diporiphora winneckeii</i>	AY133012	S4
	<i>Hypsilurus (Arua) modestus</i>	AF128464	S12
	<i>Hypsilurus boydii</i>	AY133013	S4
	<i>Hypsilurus bruijnii</i>	AY133014	S4
	<i>Hypsilurus dilophus</i>	AF128466	S12
	<i>Hypsilurus nigrigularis</i>	AY133016	S4
	<i>Hypsilurus papuensis</i>	AY133017	S4
	<i>Hypsilurus spinipes</i>	AY133018	S4
	<i>Lophognathus gilberti</i>	AY133019	S4
	<i>Lophognathus longirostris</i>	AF128462	S12
	<i>Moloch horridus</i>	AF128467	S12
	<i>Physignathus lesueurii</i>	AF128463	S12
	<i>Pogona barbata</i>	AF128474	S12
	<i>Pogona brevis</i>	AY133020	S4
	<i>Pogona henrylawsoni</i>	AY133021	S4
	<i>Pogona minima</i>	AY133022	S4
	<i>Pogona minor</i>	AY133023	S4
	<i>Pogona mitchelli</i>	AY133024	S4
	<i>Pogona nullarbor</i>	AY133025	S4
	<i>Pogona vitticeps</i>	AY133026	S4
	<i>Rankinia diemensis</i>	AF375619	S3
	<i>Tympanocryptis centralis</i>	AY133030	S4
	<i>Tympanocryptis cephalus</i>	AY133027	S4
	<i>Tympanocryptis houstoni</i>	AY133028	S4
	<i>Tympanocryptis intima</i>	AY133029	S4
	<i>Tympanocryptis lineata</i>	AF128475	S12
	<i>Tympanocryptis pinguicolla</i>	AY133031	S4
<i>Tympanocryptis tetraporophora</i>	AY133032	S4	
<b>Phrynosomatines</b>	<i>Callisaurus draconoides</i>	AY297492	
	<i>Cophosaurus texanus</i>	AY297489	
	<i>Holbrookia maculata</i>	AY297490	

<b>Taxon</b>	<b>Species</b>	<b>Accession number</b>	<b>Reference</b>
<b>Phrynosomatines</b>	<i>Holbrookia propinqua</i>	AY297491	
	<i>Petrosaurus mearnsi</i>	L40444; L41450	S13
	<i>Petrosaurus thalassinus</i>	AF049858	S14
	<i>Phrynosoma asio</i>	L40446; L41452	S13
	<i>Phrynosoma cornutum</i>	AY297487	
	<i>Phrynosoma coronatum</i>	AY297485	
	<i>Phrynosoma hernandesi</i>	U82686	S15
	<i>Phrynosoma mcallii</i>	AY297486	
	<i>Phrynosoma modestum</i>	AY297484	
	<i>Phrynosoma platyrhinos</i>	AY297488	
	<i>Phrynosoma solare</i>	AF528739	S16
	<i>Phrynosoma taurus</i>	AF346844	S17
	<i>Sator angustus</i>	AF049859	S14
	<i>Sceloporus adleri</i>	AY297519	
	<i>Sceloporus bicanthalis</i>	AF000800; AF000840	S18
	<i>Sceloporus carinatus</i>	AY297496	
	<i>Sceloporus cautus</i>	AY297522	
	<i>Sceloporus chrysostictus</i>	L40451; L41458	S13
	<i>Sceloporus clarkii</i>	AY297511	
	<i>Sceloporus cyanogenys</i>	AY297524	
	<i>Sceloporus dugesii</i>	L40454; L41461	S13
	<i>Sceloporus formosus</i>	AY297498	
	<i>Sceloporus graciosus</i>	AF049860	S14
	<i>Sceloporus grammicus</i>	AY297509	
	<i>Sceloporus horridus</i>	AF000804; AF000844	S18
	<i>Sceloporus hunsakeri</i>	AY297506	
	<i>Sceloporus insignis</i>	AF000806; AF000846	S18
	<i>Sceloporus jalapae</i>	AY297504	
	<i>Sceloporus jarrovii</i>	AY297512	
	<i>Sceloporus licki</i>	AF000808; AF000848	S18
	<i>Sceloporus lundelli</i>	AY297499	
	<i>Sceloporus maculosus</i>	AY297501	
	<i>Sceloporus magister</i>	AF528741	S16
	<i>Sceloporus malachiticus</i>	AY297518	
	<i>Sceloporus megalepidurus</i>	AF000822; AF000862	S18
	<i>Sceloporus melanorhinus</i>	AF000812; AF000852	S18
	<i>Sceloporus merriami</i>	AY297520	
	<i>Sceloporus mucronatus</i>	AY297497	
	<i>Sceloporus occidentalis</i>	AY297515	
	<i>Sceloporus ochoterenae</i>	AF528743	S16
	<i>Sceloporus olivaceus</i>	AY297521	
	<i>Sceloporus orcutti</i>	AY297508	
<i>Sceloporus ornatus</i>	AY297523		

<b>Taxon</b>	<b>Species</b>	<b>Accession number</b>	<b>Reference</b>	
<b>Phrynosomatines</b>	<i>Sceloporus parvus</i>	AF000792; AF000832	S18	
	<i>Sceloporus pictus</i>	AY297500		
	<i>Sceloporus poinsettii</i>	AY297510		
	<i>Sceloporus pyrocephalus</i>	AY297502		
	<i>Sceloporus scalaris</i>	AF528742	S16	
	<i>Sceloporus siniferus</i>	AY297494		
	<i>Sceloporus smaragdinus</i>	AY297517		
	<i>Sceloporus spinosus</i>	AY297525		
	<i>Sceloporus squamosus</i>	AY297495		
	<i>Sceloporus taeniocnemis</i>	L41426; L41476	S13	
	<i>Sceloporus teapensis</i>	AY297505		
	<i>Sceloporus torquatus</i>	AF000827; AF000867	S18	
	<i>Sceloporus undulatus</i>	AY297514		
	<i>Sceloporus utiformis</i>	AF528740	S16	
	<i>Sceloporus variabilis</i>	AY297507		
	<i>Sceloporus virgatus</i>	AY297516		
	<i>Sceloporus woodi</i>	AY297513		
	<i>Sceloporus zosteromus</i>	AY297503		
	<i>Uma scoparia</i>	AF049861	S14	
	<i>Urosaurus graciosus</i>	AF049862	S14	
	<i>Urosaurus microscutatus</i>	L41434; L41485	S13	
	<i>Urosaurus nigricaudus</i>	L41435; L41486	S13	
	<i>Urosaurus ornatus</i>	AY297493		
	<i>Uta palmeri</i>	L41437; L41488	S13	
	<i>Uta stansburiana</i>	AF049863	S14	
	<b>Liolaemus</b>	<i>Liolaemus abaucan</i>	AF099263	S5
		<i>Liolaemus albiceps</i>	AF099267	S5
<i>Liolaemus alticolor</i>		AF099218	S5	
<i>Liolaemus andinus</i>		AF099251	S5	
<i>Liolaemus audituvelatus</i>		AF305792		
<i>Liolaemus austromendocinus</i>		AF099239	S5	
<i>Liolaemus bellii</i>		AF099223	S5	
<i>Liolaemus bibronii</i>		AF099221	S5	
<i>Liolaemus bitaeniatus</i>		AF099219	S5	
<i>Liolaemus boulengeri</i>		AF099275	S5	
<i>Liolaemus buergeri</i>		AF099236	S5	
<i>Liolaemus canqueli</i>		AY297536		
<i>Liolaemus chacoensis</i>		AF099270	S5	
<i>Liolaemus chiliensis</i>		AF099224	S5	
<i>Liolaemus coeruleus</i>		AF099217	S5	
<i>Liolaemus cuyanus</i>		AF099252	S5	
<i>Liolaemus cyanogaster</i>		AF099225	S5	
<i>Liolaemus darwini</i>		AF099274	S5	
<i>Liolaemus dorbignyi</i>		AF099248	S5	
<i>Liolaemus elongatus</i>		AF099240	S5	
<i>Liolaemus famatinae</i>		AF099246	S5	
<i>Liolaemus fitzingerii</i>		AF099253	S5	

<b>Taxon</b>	<b>Species</b>	<b>Accession number</b>	<b>Reference</b>
<b><i>Liolaemus</i></b>	<i>Liolaemus fuscus</i>	AF099232	S5
	<i>Liolaemus gracilis</i>	AF099222	S5
	<i>Liolaemus gravenhorstii</i>	AY297527	
	<i>Liolaemus hernani</i>	AY297529	
	<i>Liolaemus huacahuasicus</i>	AY297533	
	<i>Liolaemus irregularis</i>	AF099268	S5
	<i>Liolaemus koslowskyi</i>	AF099264	S5
	<i>Liolaemus kriegi</i>	AY297530	
	<i>Liolaemus laurenti</i>	AF099273	S5
	<i>Liolaemus lemniscatus</i>	AF099229	S5
	<i>Liolaemus leopardinus</i>	AF099235	S5
	<i>Liolaemus lineomaculatus</i>	AF099241	S5
	<i>Liolaemus lutzae</i>	AF099255	S5
	<i>Liolaemus magellanicus</i>	AF099243	S5
	<i>Liolaemus melanops</i>	AF099261	S5
	<i>Liolaemus monticola</i>	AF099230	S5
	<i>Liolaemus multicolor</i>	AF099250	S5
	<i>Liolaemus multimaculatus</i>	AF099257	S5
	<i>Liolaemus nigromaculatus</i>	AY297526	
	<i>Liolaemus nigroviridis</i>	AF099233	S5
	<i>Liolaemus nitidus</i>	AF099231	S5
	<i>Liolaemus occipitalis</i>	AF099256	S5
	<i>Liolaemus olongasta</i>	AF099271	S5
	<i>Liolaemus orientalis</i>	AF099247	S5
	<i>Liolaemus ornatus</i>	AF099266	S5
	<i>Liolaemus paulinae</i>	AY297531	
	<i>Liolaemus petrophilus</i>	AF099238	S5
	<i>Liolaemus pictus</i>	U82684	S15
	<i>Liolaemus platei</i>	AY297528	
	<i>Liolaemus poecilochromus</i>	AF099249	S5
	<i>Liolaemus pseudoanomalus</i>	AF099254	S5
	<i>Liolaemus quilmes</i>	AF099265	S5
	<i>Liolaemus riojanus</i>	AY297534	
	<i>Liolaemus robertmertensi</i>	AF099220	S5
	<i>Liolaemus rothi</i>	AF099262	S5
	<i>Liolaemus ruibali</i>	AF099244	S5
	<i>Liolaemus salinicola</i>	AF099259	S5
	<i>Liolaemus scapularis</i>	AF099258	S5
	<i>Liolaemus schroederi</i>	AF305791	
	<i>Liolaemus somuncurae</i>	AF099242	S5
	<i>Liolaemus stolzmanni</i>	AY297532	
	<i>Liolaemus tenuis</i>	AF099228	S5
<i>Liolaemus uspallatensis</i>	AF099269	S5	
<i>Liolaemus walkeri</i>	AF305790		
<i>Liolaemus wiegmanni</i>	AF099260	S5	
<i>Liolaemus xanthoviridis</i>	AY297535		
<i>Liolaemus zapallarensis</i>	AF099227	S5	

<b>Taxon</b>	<b>Species</b>	<b>Accession number</b>	<b>Reference</b>
<b><i>Anolis</i></b>	<i>Anolis acutus</i>	AF055926	S1
	<i>Anolis aeneus</i>	AF055950	S1
	<i>Anolis ahli</i>	AY296148	S19
	<i>Anolis alayoni</i>	AY296149	S19
	<i>Anolis alfaroi</i>	AY296150	S19
	<i>Anolis aliniger</i>	AF055959	S1
	<i>Anolis allisoni</i>	AY296151	S19
	<i>Anolis allogus</i>	AY296152	S19
	<i>Anolis alumina</i>	AY296153	S19
	<i>Anolis alutaceus</i>	AF055971	S1
	<i>Anolis angusticeps</i>	AF055967	S1
	<i>Anolis argenteolus</i>	AY296154	S19
	<i>Anolis armouri</i>	AY263012	S20
	<i>Anolis bahorucoensis</i>	AF055932	S1
	<i>Anolis baleatus</i>	AY296155	S19
	<i>Anolis baracoae</i>	AY296156	S19
	<i>Anolis barahonae</i>	AF055972	S1
	<i>Anolis bartschi</i>	AF055960	S1
	<i>Anolis bimaculatus</i>	AF055930	S1
	<i>Anolis bremeri</i>	AY296157	S19
	<i>Anolis brevirostris</i>	AY296158	S19
	<i>Anolis brunneus</i>	AY296159	S19
	<i>Anolis carolinensis</i>	AF294279	S21
	<i>Anolis caudalis</i>	AY296161	S19
	<i>Anolis centralis</i>	AY296162	S19
	<i>Anolis chlorocyanus</i>	AY296163	S19
	<i>Anolis christophei</i>	AF055957	S1
	<i>Anolis coelestinus</i>	AY296164	S19
	<i>Anolis conspersus</i>	AF294304	S21
	<i>Anolis cooki</i>	AY296165	S19
	<i>Anolis cristatellus</i>	AY296166	S19
	<i>Anolis cuvieri</i>	AF055973	S1
	<i>Anolis cybotes</i>	AY263133	S20
	<i>Anolis desechensis</i>	AY296167	S19
	<i>Anolis distichus</i>	AY296168	S19
	<i>Anolis dolichocephalus</i>	AY296169	S19
	<i>Anolis equestris</i>	AF055978	S1
	<i>Anolis ernestwilliamsi</i>	AY296170	S19
	<i>Anolis etheridgei</i>	AF055934	S1
	<i>Anolis eugenegrahami</i>	AY296171	S19
	<i>Anolis evermanni</i>	AY296172	S19
	<i>Anolis ferreus</i>	AY296173	S19
	<i>Anolis fowleri</i>	AY296174	S19
	<i>Anolis garmani</i>	AF294289	S21
	<i>Anolis garridoi</i>	AY296175	S19
	<i>Anolis grahami</i>	AF294299	S21
	<i>Anolis griseus</i>	AY296176	S19
	<i>Anolis gundlachi</i>	AY296177	S19

<b>Taxon</b>	<b>Species</b>	<b>Accession number</b>	<b>Reference</b>
<b><i>Anolis</i></b>	<i>Anolis haetianus</i>	AY263042	S20
	<i>Anolis hendersoni</i>	AY296178	S19
	<i>Anolis homolechis</i>	AY296179	S19
	<i>Anolis imias</i>	AF294314	S21
	<i>Anolis inexpectatus</i>	AY296180	S19
	<i>Anolis insolitus</i>	AF055933	S1
	<i>Anolis isolepis</i>	AY296181	S19
	<i>Anolis jubar</i>	AY296182	S19
	<i>Anolis krugi</i>	AF055928	S1
	<i>Anolis leachii</i>	AY296183	S19
	<i>Anolis lineatopus</i>	AF294295	S21
	<i>Anolis longiceps</i>	AY296184	S19
	<i>Anolis longitibialis</i>	AY263010	S20
	<i>Anolis loysianus</i>	AF055964	S1
	<i>Anolis luciae</i>	AF055951	S1
	<i>Anolis lucius</i>	AF055962	S1
	<i>Anolis luteogularis</i>	AF055977	S1
	<i>Anolis macilentus</i>	AY296185	S19
	<i>Anolis marcanoii</i>	AY263006	S20
	<i>Anolis marmoratus</i>	AY296186	S19
	<i>Anolis marron</i>	AY296187	S19
	<i>Anolis maynardi</i>	AF055969	S1
	<i>Anolis mestrei</i>	AF337779	S19
	<i>Anolis monensis</i>	AY296188	S19
	<i>Anolis monticola</i>	AY296189	S19
	<i>Anolis noblei</i>	AY296190	S19
	<i>Anolis occultus</i>	AF055976	S1
	<i>Anolis oculatus</i>	AY296191	S19
	<i>Anolis olssoni</i>	AF055945	S1
	<i>Anolis opalinus</i>	AF294305	S21
	<i>Anolis ophiolepis</i>	AF055942	S1
	<i>Anolis paternus</i>	AF055965	S1
	<i>Anolis placidus</i>	AY296192	S19
	<i>Anolis pogus</i>	AY296193	S19
	<i>Anolis poncensis</i>	AY296194	S19
	<i>Anolis porcatus</i>	AY296195	S19
	<i>Anolis pulchellus</i>	AY296196	S19
	<i>Anolis pumilus</i>	AF055963	S1
	<i>Anolis quadriocellifer</i>	AY296197	S19
	<i>Anolis reconditus</i>	AY296198	S19
	<i>Anolis richardi</i>	AF055949	S1
<i>Anolis roquet</i>	AY296199	S19	
<i>Anolis sagrei</i>	AF337778	S19	
<i>Anolis scriptus</i>	AY296200	S19	
<i>Anolis semilineatus</i>	AY296201	S19	
<i>Anolis sheplani</i>	AF055966	S1	
<i>Anolis shrevei</i>	AY263036	S20	
<i>Anolis singularis</i>	AY296202	S19	

<b>Taxon</b>	<b>Species</b>	<b>Accession number</b>	<b>Reference</b>
<b><i>Anolis</i></b>	<i>Anolis smallwoodi</i>	AY296203	S19
	<i>Anolis smaragdinus</i>	AF055968	S1
	<i>Anolis strahmi</i>	AY263008	S20
	<i>Anolis stratulus</i>	AF055929	S1
	<i>Anolis trinitatis</i>	AY296204	S19
	<i>Anolis valencienni</i>	AF294310	S21
	<i>Anolis vanidicus</i>	AF055970	S1
	<i>Anolis vermiculatus</i>	AF055961	S1
	<i>Anolis wattsi</i>	AF055931	S1
	<i>Anolis websteri</i>	AY296205	S19
	<i>Anolis whitemani</i>	AY263024	S20
	<i>Chamaeleolis barbatus</i>	AY296146	S19
	<i>Chamaelinorops barbouri</i>	AF055946	S1
	<i>Chamaeleolis chamaeleonides</i>	AF055975	S1
	<i>Chamaeleolis guamuhaya</i>	AF055974	S1
	<i>Chamaeleolis porcus</i>	AY296147	S19

Table S2. Average coefficients of variation, with standard deviations, over all variables for each lizard taxon included in this study.

<b>Clade</b>	<b>Average coefficient of variation (<math>\pm</math> sd)</b>
<b>Australian Agamids</b>	0.183 $\pm$ 0.055
<b>Phrynosomatines</b>	0.141 $\pm$ 0.044
<b><i>Liolaemus</i></b>	0.101 $\pm$ 0.039
<b><i>Anolis</i></b>	0.212 $\pm$ 0.264

**References:**

- S1. T. R. Jackman, A. Larson, K. de Queiroz, J. B. Losos, *Syst. Biol.* **48**, 254 (1999).
- S2. J. A. Schulte II, *A Phylogenetic and Ecological Analysis of Iguanian Lizard Evolution*, thesis, Washington University (2001).
- S3. J. Melville, J. A. Schulte II, A. Larson, *J. Exp. Zool.* **291**, 339 (2001).
- S4. J. A. Schulte II, J. Melville, A. Larson, *Proc. R. Soc. London Ser. B* **270**, 597 (2003).
- S5. J. A. Schulte II, J. R. Macey, R. E. Espinoza, A. Larson, *Biol. J. Linn. Soc.* **69**, 75 (2000).
- S6. J. J. Wiens, *Syst. Biol.* **47**, 427 (1998).
- S7. D. Posada, K. A. Crandall, *Bioinformatics* **14**, 817 (1998).
- S8. D. L. Swofford, *PAUP\*: Phylogenetic Analysis Using Parsimony (\*and Other Methods)* (Sinauer, New York, 2002).
- S9. M. J. Sanderson, *Mol. Biol. Evol.* **14**, 1218 (1997).
- S10. A. Rambaut and M. Charleston, TreeEdit version 1.0 alpha 4-61 (<http://evolve.zoo.ox.ac.uk/software/TreeEdit/main.html>) (2000).
- S11. A. Rambaut., PhyloGen version 1.1 (<http://evolve.zoo.ox.ac.uk/software/PhyloGen/main.html>) (2001).
- S12. J. R. Macey *et al.*, *Syst. Biol.* **49**, 233 (2000).
- S13. T. W. Reeder, *Mol. Phylogenet. Evol.* **4**, 203 (1995).
- S14. J. A. Schulte II, J. R. Macey, A. Larson, and T. J. Papenfuss, *Mol. Phylogenet. Evol.* **10**, 367 (1998).
- S15. J. R. Macey, A. Larson, N. B. Ananjeva, T. J. Papenfuss, *J. Mol. Evol.* **44**, 660 (1997).
- S16. J. A. Schulte II, J. P. Valladares, A. Larson, *Herpetologica*, in press.

- S17. T. W. Reeder, R. R. Montanucci, *Copeia* **2001**, 309 (2001).
- S18. J. J. Wiens, T. W. Reeder, *Herpetological Monographs* **11**, 1 (1997).
- S19. J. B. Losos, M. Leal, R. E. Glor, K. de Queiroz, P. E. Hertz, L. Rodríguez Schettino, A. Chamizo Lara, T. R. Jackman, A. Larson, *Nature* **424**, 542 (2003).
- S20. R. E. Glor, J. J. Kolbe, R. Powell, A. Larson, J. B. Losos, *Evolution*, in press.
- S21. T. R. Jackman, D. J. Irschick, K. de Queiroz, J. B. Losos, A. Larson, *J. Exp. Zool.* **294**, 1 (2002).